PNAS
www.pnas.org

Main Manuscript for

Root angle is controlled by *EGT1* in cereal crops employing a novel anti-gravitropic mechanism.

Riccardo Fusi[1,2,#], Serena Rosignoli[3,#], Haoyu Lou[1,4,5,#], Giuseppe Sangiorgi[3], Riccardo Bovina[3], Jacob K. Pattem[6], Aditi N. Borkar[7,8], Marco Lombardi[1,9], Cristian Forestan[3], Sara G. Milner[3], Jayne L. Davis[1], Aneesh Lale[1,2], Gwendolyn K. Kirschner[10], Ranjan Swarup[1], Alberto Tassinari[3], Bipin K. Pandey[1,2], Larry M. York[1,11], Brian S. Atkinson[1], Craig J. Sturrock[1], Sacha J. Mooney[1], Frank Hochholdinger[10], Matthew R. Tucker[4,5], Axel Himmelbach[12], Nils Stein[12,13], Martin Mascher[12,14], Kerstin A. Nagel[15], Laura De Gara[9], James Simmonds[16], Cristobal Uauy[16], Roberto Tuberosa[3], Jonathan P. Lynch[1,17], Gleb E. Yakubov[6], Malcolm J. Bennett[1,2,*], Rahul Bhosale[1,2,*] & Silvio Salvi[3,*]

[1]School of Biosciences, University of Nottingham, Sutton Bonington Campus, LE12 5RD, UK

[2]Future Food Beacon of Excellence, University of Nottingham, Sutton Bonington Campus, LE12 5RD, UK

[3]Department of Agricultural and Food Sciences, University of Bologna, Viale Fanin 44, 40127 Bologna, Italy

[4]School of Agriculture, Food and Wine, Waite Research Institute, The University of Adelaide, Glen Osmond, SA 5062, Australia

[5]Australian Research Council Centre of Excellence in Plant Cell Walls, The University of Adelaide, Glen Osmond, SA 5062, Australia

[6]Food Sciences, University of Nottingham, Sutton Bonington, LE12 5RD UK

[7]School of Veterinary Medicine and Science, University of Nottingham, Sutton Bonington, LE12 5RD UK

[8]Wolfson Center for Global Virus Research, University of Nottingham, UK

[9] Department of Science and Technology for Humans and the Environment, Campus Bio-Medico University of Rome, Rome, 00128, Italy

[10]Institute of Crop Sciences and Resource Conservation (INRES), Crop Functional Genomics, University of Bonn, 53113 Bonn, Germany

[11]Biosciences Division, Oak Ridge National Laboratory, Oak Ridge, TN 37830, USA

[12]Leibniz Institute of Plant Genetics and Crop Plant Research (IPK) Gatersleben, Seeland, Germany

[13]Center of integrated Breeding Research (CiBreed), Department of Crop Sciences, Georg-August-University, Von Siebold Str. 8, 37075 Göttingen, Germany

[14]German Centre for Integrative Biodiversity Research (iDiv) Halle-Jena-Leipzig, Leipzig, Germany

[15]Institute of Bio- and Geo-sciences, Plant Sciences (IBG-2), Forschungszentrum Juelich, Germany

[16]John Innes Centre, Norwich Research Park, Norwich NR4 7UH, UK

[17]Department of Plant Science, The Pennsylvania State University, University Park, PA 16802, USA

[#]These authors contributed equally to this work.

*__Corresponding authors__: Malcolm Bennett, Rahul Bhosale & Silvio Salvi

Email: malcolm.bennett@nottingham.ac.uk, rahul.bhosale@nottingham.ac.uk and silvio.salvi@unibo.it

Author Contributions: M.J.B., Ra.B., and S.S. designed research; R.F., S.R., H.L., G.S., Ri.B., J.K.P., A.N.B., M.L., C.F., S.G.M., J.L.D, A.L., G.K.K., R.S., A.T., B.K.P., L.M.Y., B.S.A., C.J., A.H. and Ra.B. performed experiments and analysed data. S.J.M., F.H., M.R.T., N.S., M.M., K.A.N., L.D.G., J.S., C.U., R.T., J.P.L and G.E.Y. provided material and resources. R.F., S.R., H.L., M.J.B., Ra.B., and S.S. wrote the manuscript. All authors read and edited manuscript.

Competing Interest Statement: The authors declare no competing interests.

Classification: Biological sciences, Plant Biology

Keywords: root angle, anti-gravitropic, cell-wall, barley, wheat

This PDF file includes:

Main Text
Figures 1 to 4

Abstract

Root angle in crops represents a key trait for efficient capture of soil resources. Root angle is determined by competing gravitropic versus anti-gravitropic offset (AGO) mechanisms. Here we report a new root angle regulatory gene termed *ENHANCED GRAVITROPISM1* (*EGT1*) that encodes a putative AGO component, whose loss of function enhances root gravitropism. Mutations in barley and wheat *EGT1* genes confer a striking root phenotype, where every root class adopts a steeper growth angle. *EGT1* encodes a F-box and Tubby domain containing protein which is highly conserved across plant species. Haplotype analysis found that natural allelic variation at the barley *EGT1* locus impacts root angle. Gravitropic assays indicated that *Hvegt1* roots bend more rapidly than wildtype. Transcript profiling revealed *Hvegt1* roots deregulate ROS homeostasis and cell wall-loosening enzymes and cofactors. ROS imaging shown that *Hvegt1* root basal meristem and elongation zone tissues have reduced levels. Atomic Force Microscopy measurements detected elongating *Hvegt1* root cortical cell walls are significantly less stiff than wildtype. *In situ* analysis identified *HvEGT1* is expressed in elongating cortical and stele tissues, which are distinct from known root gravitropic perception and response tissues in the columella and epidermis, respectively. We propose that EGT1 controls root angle by regulating cell wall stiffness in elongating root cortical tissue, counteracting the gravitropic machinery's known ability to bend the root via its outermost tissues. We conclude that root angle is controlled by *EGT1* in cereal crops employing a novel anti-gravitropic mechanism.

Significance Statement

The growth angle roots adopt are critical for capturing soil resources such as nutrients and water. Despite its agronomic importance, few regulatory genes have been identified in crops. Here we identify the novel root angle regulatory gene *ENHANCED GRAVITROPISM 1 (EGT1)* in barley. Strikingly, mutants lacking *EGT1* exhibit a steeper angle in every root class. EGT1 appears to function as a component of a novel anti-gravitropic offset mechanism that regulates tissue stiffness which impacts final root growth angle. *EGT1* is a hot spot for selection as natural allelic variation within a conserved Tubby domain is linked with steeper root angle. Analogous *EGT1* dependent regulation of root angle in wheat demonstrates broad significance of EGT1 for trait improvement in cereal crops.

Main Text

Introduction

Root architectural traits such as angle plays a critical role in adapting to different environmental conditions and capturing soil resources such as water and nutrients. For instance, deeper root growth angle is advantageous for accessing subsoil water and enhancing drought tolerance and improving Nitrogen (N) capture, while shallow root growth angle improves capture of phosphorus (P) from topsoil (1–3). Moreover, recent studies report that modified root angle increases yield under saline conditions (4). Thus, improved understanding of the genes and mechanisms controlling root growth angle would facilitate breeding of crop varieties better suited for different abiotic stresses arising from future climatic conditions.

The growth angles of different root classes (e.g., primary, seminal, lateral and crown) are often distinct to limit competition. These distinct angles are referred to as gravitropic setpoint angle (GSA). The GSA of different root classes is determined by competing gravitropic and anti-gravitropic offset (AGO) mechanisms (5, 6). The gravitropic mechanism has been extensively studied in *Arabidopsis thaliana* roots. These studies have identified that changes in root orientation is perceived in columella cells at the root tip, triggering formation of a lateral auxin

gradient which root cap cells transport to epidermal cells in the elongation zone, leading to differential root growth and bending (7–9). In contrast to the detailed knowledge about the genes, signals and mechanisms involved in the root gravitropic response, the AGO mechanism(s) is only recently beginning to be unraveled (5, 6). Auxin transport has also been linked with the AGO mechanism, implying that the interaction of two opposing gravitropic and AGO regulated auxin fluxes could determine the angle of organ growth (10, 11). However, detailed knowledge about auxin-dependent or auxin-independent components of AGO mechanism(s) still remains unclear.

Here, we report a novel putative component of the AGO mechanism in cereal roots termed *ENHANCED GRAVITROPISM 1* (*EGT1*). Screening of a barley TILLING mutant collection identified a mutant exhibiting a striking steep root growth angle phenotype. Bulk-segregant analysis mapped the mutation within a 130 Mb region on chromosome 6. Exome and WGS sequencing identified mutations in the coding sequence of *HORVU6Hr1G068970* (Tubby-like F-box protein). TILLING studies revealed EGT1 function is also conserved in durum wheat. *HvEGT1* is highly expressed in root stele tissues distinct from known auxin-mediated gravity responsive root cap and epidermal tissues. *HvEGT1* appears to function in a novel auxin independent AGO mechanism. RNA sequencing revealed many peroxidases and cell wall softening/stiffening enzymes are differentially regulated in *hvegt1* mutant root tips compared to wildtype. Atomic Force Microscopy measurements revealed elongation zone cell walls of *Hvegt1* roots are significantly less stiff than wildtype. We propose that *HvEGT1* controls root growth angle by functioning as an AGO component in an auxin-independent pathway in elongating root tissues, via regulation of cell wall stiffening and loosening, thereby serving to counteract gravitropic bending in the outermost tissues.

Results

Barley mutant TM194 exhibits steeper root growth angle in every root class

A barley root mutant line TM194 exhibiting a striking steeper seminal and lateral root phenotype (Fig. S1) was initially identified in a chemically mutagenized population of the cv. Morex (12) using a semi-hydroponic rhizotron screening system. 3D root architecture phenotyping of 10-days old TM194 roots using X-ray micro–Computed Tomography (CT) (13) revealed the steeper seminal root angle phenotype directly in soil (Fig. 1a). Phenotyping TM194 roots 20-days after germination (using soil-filled rhizotrons) and at grain maturation stage (using microCT) revealed lateral and crown root angles are also significantly steeper compared to wildtype Morex (Fig. 1b-d). Hence, the TM194 mutant exhibited steeper root growth angle in every root class examined, in both semi-hydroponic and soil conditions. In contrast, no significant difference in shoot growth angle (*P-value* 0.4819, Fig. S2a) at seedling stage or leaf growth angle (*P-value* 0.566, Fig. S2b) at the flowering stage was observed in the TM194 mutant compared to wildtype. Hence, the TM194 mutation causes a root specific angle defect.

TM194 root angle defect is caused by a mutation in *ENHANCED GRAVITROPISM 1* (*Hv**EGT1***)

To discover the genetic and molecular basis of the TM194 root growth angle phenotype, the mutant was initially out crossed to Barke, a distinct barley variety which exhibits a similar root growth angle phenotype to cv. Morex. Whilst F_1 plants exhibited a wildtype phenotype, F_2 plants (n = 75) segregated in a Mendelian pattern for either a steeper or wildtype seminal root phenotype (59:16 plants, wildtype vs steeper, respectively, X^2 3:1, n.s.), consistent with the TM194 root growth angle phenotype segregating as a single recessive allele. Using the same F_2 population, a SNP-based bulk segregant analysis (BSA) revealed that the mutated locus mapped to chromosome 6 (Fig. 2a), in a large pericentromeric region spanning c. 130 Mb between markers *BOPA2_12_30144* and *BOPA1_4109-90*.

To pinpoint the root angle mutation, exome sequencing was performed on TM194. This revealed missense mutations in four genes within the chromosome 6H region highlighted by BSA (Fig. 2b-c, SI Dataset 1). To pinpoint the relevant gene, we exome sequenced a second independent root angle mutant allele termed TM3580 (Fig. S3). TM3580 contained six mutations in the same chromosome region, while only one mutation coincided with TM194 in an overlapping gene *HORVU6Hr1G068970* (encoding Tubby-Like F-box Protein) (SI Dataset 1, highlighted in red). F1 progenies of a genetic cross between TM3580 and TM194 did not complement steeper root growth angle phenotype (Fig. S4), confirming that these mutants are allelic at locus *HORVU6Hr1G068970*. Specifically, TM3580 contained a mutation in the first intron of *HORVU6Hr1G068970,* predicted to cause a splice acceptor variant (SI Dataset 1). Bulk RNAseq analysis of TM3580 and Morex root samples confirmed the TM3580 mutation caused a splice acceptor variant, resulting in a deletion of 9 amino acids without any frameshift (Fig. S5). Interestingly, neither mutation significantly affects *HORVU6Hr1G068970* expression level (Fig. S6), suggesting their steeper root phenotype is due to altered HvEGT1 protein structure or function. Taken together, these results provided conclusive evidence that mutations in *HORVU6Hr1G068970* are responsible for the steeper root angle phenotype, leading us to name this gene as barley ***E****NHANCED* ***G****RAVI****T****ROPISM* ***1*** (*Hv****EGT1***).

Mutations in HvEGT1 Tubby domain disrupt gene function

Next, we examined whether nucleotide polymorphisms within *HvEGT1* could provide a source of natural variation in root growth angle observed in barley diversity panels. We exploited the availability of exome sequence of a large barley germplasm collection (WHEALBI collection) (14). Using haplotype network analysis of nucleotide sequence variation within the *HvEGT1* coding sequence, we identified two haplotypes (II and IV) carrying missense substitutions and four other haplotypes carrying synonymous substitutions (I, III, V and VI) (Fig. 2d). Based on this result, we phenotyped barley accessions carrying haplotypes II (n = 86) and IV (n = 25) using a semi-hydroponic system. Accessions carrying haplotype II exhibited significantly steeper seminal root angle distribution than accessions carrying haplotype IV (50.9 ±14.8 *vs*. 64.3 ±17.6, median ± s.d. degree angle, respectively; P <0.001) (Fig. 2e). To understand this further, we mapped their substitutions onto the HvEGT1 protein structure and compared them with the TM194 mutation. Interestingly, haplotype II causes a F391L substitution, just four amino acids away from TM194 (G395E) (Fig. S7c) and both these substitutions lie within a highly evolutionary conserved motif (position 391-400) shared by 37 plant species (Fig. S8). In contrast, haplotype IV causes a S306C substitution, 89 amino acids upstream of the TM194 mutation (Fig. S7c).

To investigate the effect of these mutations on EGT1 structure and function we constructed a homology model for Tubby and F-box domains using Phyre2 (15) (Fig. S7a-b). For example, G395 sits in a highly positively charged cavity, likely to be stabilized by an adjacent negatively charged C-terminal site. The TM194 G395E substitution causes a small, neutral amino acid to be substituted by a larger, negatively charged residue, which is likely to destabilise this region and impact protein function. Further, TM3580, a splice acceptor mutant containing a 9 amino acid deletion between residues 129 to 137, causes significant structural changes at the N-terminal region of the Tubby domain. This includes introduction of a short α-helical segment which presents amino acids with different physiochemical properties (polarity, hydrophobicity and charge) on the domain surface (Fig. S7d, h). To understand the structure-function relation of these changes, we constructed the structure of the whole EGT1 protein using *de novo* prediction from full protein sequence in Alphafold2 (16). This structure shows that the F-box domain (Fig. S7e-f) presents a part charged, part hydrophobic protein-protein interaction interface to the Tubby domain (Fig. S7e-h). While the wildtype Tubby domain complements this physiochemical presentation (Fig. S7g), the structural alterations in the TM3580 mutant leads to juxtaposition of negatively charged residues on the protein-protein interface (Fig. S7h), likely destabilising the overall structure and function of the mutant protein.

EGT1 mediated root growth angle regulation is conserved in wheat

Phylogenetic analysis of Tubby-like F-Box protein sequences in barley, wheat, rice and brachypodium identified closely related proteins in all these species (Fig. S9). To address EGT1 function in another cereal, we screened (*in-silico*) a TILLING population of tetraploid (AA BB) wheat cv. Kronos (17). Kronos2551 and Kronos3926 lines encoded premature termination codons in TRITD6Bv1G159700 (*HvEGT1* homoeologous gene on wheat B genome) and the Kronos2708 line carrying a splice donor mutation in TRITD6Av1G172130 (*HvEGT1* homoeologous gene on wheat A genome). Kronos2551 × Kronos2708 and Kronos3926 × Kronos2708 were crossed, then F1 plants were self-pollinated to create F2 plants. Progenies of selected wildtype and homozygous double mutants from two independent crosses were grown for seven days in rhizoboxes for root growth angle analysis. Both the double mutants exhibited steeper seminal and lateral root growth angle compared with the progenies carrying wildtype alleles in both homologs as well as homozygous mutations in just one homolog (Fig. S10). Hence, our results revealed that *TdEGT1* loci also control root growth angle in wheat and possibly other cereal and plant species.

HvEGT1 controls root growth angle via an anti-gravitropic offset (AGO) mechanism

Different root classes adopt specific gravitropic setpoint angles (GSA), which are maintained by competing gravitropic and anti-gravitropic offset (AGO) mechanisms (11, 18). Lugol staining of *Hvegt1* (TM194) mutant root tips revealed no observable differences in starch granule accumulation in statolith organelles, suggesting the root gravity sensing machinery remains intact in the mutant (Fig. S11). In *Hvegt1* mutants, seminal, lateral and crown roots are no longer able to maintain their non-vertical GSA, suggesting *HvEGT1* operates as part of the AGO pathway. To validate this, we compared root bending responses of four-day old seminal roots in *Hvegt1* (TM194) and Morex after either a 30º, 60º or 90º gravistimulus (Fig. 3a). If the gravitropic mechanism was compromised in *Hvegt1*, its root bending rate would be slower. In contrast, if the AGO mechanism was compromised in *Hvegt1,* the countering gravitropic mechanism would confer a higher bending rate. Our results revealed *Hvegt1* roots exhibited a significantly higher bending angle and faster gravitropic response than Morex even after 0.5 hour at a 30º tilting gravistimulus and this difference became even more exaggerated with increasing tilting angle (Fig. 3b). Hence, the *Hvegt1* mutant appears disrupted in its anti-gravitropic (rather than gravitropic) response, consistent with *HvEGT1* encoding a putative component of the AGO mechanism.

HvEGT1 appears to function as part of an auxin-independent AGO mechanism

Auxin transport and response has been reported to play a role in both gravitropic and AGO mechanisms (11, 19–22), as exogenous application of auxin or auxin transport inhibitor influences GSA. We tested whether the *HvEGT1* expression and gravitropic bending response of *Hvegt1* mutant was influenced by exogenous auxin and auxin inhibitor treatment. RT-qPCR analysis revealed *HvEGT1* expression was not significantly induced after 10 nM NAA and 1 µM NPA treatments in either Morex (*P-values* 0.0655 and 0.0818, respectively) or TM194 mutant (*P-values* 0.06176 and 0.1176, respectively) backgrounds (Fig. S12). In contrast, auxin inducible gene *HvIAA36 and HVIAA22* (23) showed a significant induction, both in Morex (*P-value* 0.0461 and 0.0423) and TM194 mutant (*P-value* 0.0256 and 0.0360), suggesting that *HvEGT1* expression is auxin independent. Additionally, transcription factor binding site prediction tool PlantRegMap (24) did not identify any auxin response elements (AuxRE), which are required for auxin dependent expression regulation within the 2.5kb promoter of *HvEGT1* (SI Dataset 2). Similarly, root bending response at 0.5, 3, 9, 12 and 24 hours after a 90º gravistimulus and NPA treatment significantly reduced root bending velocity to similar degrees in both mutant and wildtype, while no significant change was observed for NAA treatment (Fig. 3c-d). This indicated that the auxin-mediated gravitropic response mechanism remains intact in *Hvegt1*. Consistently,

our root RNAseq dataset did not show overrepresentation of auxin signaling genes in either *Hvegt1* mutant alleles compared to wildtype (Fig. 4a, SI Dataset 3-4). Further, detailed comparative expression analysis of auxin transport and biosynthesis genes showed that auxin signaling pathway in both mutant alleles remain mostly unperturbed when compared to Morex (SI Dataset 5). Taken together, our root bioassays, promoter analysis and RNAseq results suggest that *HvEGT1* functions as part of an auxin-independent AGO mechanism.

Mutations in *HvEGT1* deregulates expression of ROS homeostasis and cell wall enzymes

To determine why *Hvegt1* roots bend more rapidly than wildtype, we analysed root transcript profiles to reveal which classes of genes were differentially expressed. In total, 6443 genes were identified to be differentially expressed (Benjamini-Hochberg FDR corrected p-value < 0.05, -1.5<FC>1.5 and FPKM > 1) between comparisons of TM194 *vs* Morex, TM3580 *vs* Morex and TM194 *vs* TM3580 (SI Dataset 3). We focused on the 841 differentially expressed genes in both *Hvegt1* mutant alleles compared to Morex. GO enrichment identified overrepresentation for mainly hydrogen-peroxide and cell wall related biological processes (Fig. 4a, SI Dataset 4). Interestingly, hydrogen peroxide catabolic and metabolic processes were explicitly enriched by 21 cell wall peroxidases (SI Dataset 6). This suggested that *Hvegt1* mutant alleles may have differences in ROS homeostasis compared to Morex. Consistently, ROS detection assays using CM-H_2DCFDA revealed that the *Hvegt1* (*TM194)* mutant, when compared to Morex, has a reduced level of ROS in root tips and it explicitly in the root meristem and elongation zone (Fig. S13). Peroxidases are associated with cell wall loosening and stiffening processes through ROS for oxidative polymerisation of cell wall aromatic compounds within phenolics or oxidative scission of cell wall polysaccharides (cellulose, hemicellulose e.g., xyloglucans and pectins (25). Consistently, we observed that cell wall organisation or biogenesis, including xyloglucan metabolic processes, were enriched by 23 genes encoding cell wall-modifying enzymes (i.e., expansins, chitinase family proteins, glucosyltransferases, pectin methylesterase inhibitors, fasciclin-like arabinogalactan proteins and xyloglucan hydrolases) (SI Dataset 6). Many of these enzymes modify cell wall components during growth and development (26, 27). Co-expression analysis with published barley RNAseq data (28) further indicated that several cell wall gene modules were differentially expressed in *hvegt1* versus wildtype roots (Fig. S14). The spatio-temporal expression enrichment of orthologs of these peroxidases and cell wall in rice roots (29, 30) revealed that the majority are mostly expressed in stele tissues of proximal meristem and elongation zones (Fig. S15).

***HvEGT1* is highly expressed in expanding root tissues**

To determine the site of action of *HvEGT1*, we elucidated its spatial expression in root tissues using RNA In-Situ Hybridisation (ISH) (31). A *HvEGT1* specific, non-conserved region (compared to other barley Tubby genes) spanning the end of CDS and the start of 3' UTR was used to design and synthesise digoxigenin-labelled antisense and sense probes (Fig. S16). *In situ* hybridised longitudinal and radial root sections revealed the *HvEGT1* transcript is most highly abundant in basal meristem and transition zone cells (Fig 4b-c, Fig. S17). No major difference was detected for *HvEGT1* transcript in *in situ* hybridised roots of TM194 mutant compared to Morex (Fig. S18), consistent with our RNAseq and qPCR results (Fig. S6). The level of *HvEGT1* expression then decreased until it became undetectable in maturation zone cells. The hybridized cross sections revealed highest *HvEGT1* transcript levels in stele and cortical tissues in the basal meristem and elongation zones. In contrast, sections through the apical meristem showed only a weak signal (Fig. 4d-f). Hence, *HvEGT1* expression is primarily associated with root cells starting to elongate, consistent with the spatio-temporal expression of the classes of genes identified to be differentially regulated in our *Hvegt1 vs* wildtype RNAseq analysis (Fig. S15). The enriched pattern of EGT1 expression (and differentially expressed ROS and cell wall genes) in stele and cortical root elongation zone tissues is distinct from the outermost tissues known to be involved in root gravitropic bending response (32).

Atomic Force Spectroscopy suggests *Hvegt1* mutants have less stiff root cell walls

Given that loss of *HvEGT1* deregulates genes encoding cell wall modifying enzymes, we examined whether EGT1 regulates cell wall properties and hence cell wall stiffness. To test this hypothesis, we analysed 50 µM thick longitudinal cross-sections of 4-day-old seminal root tips of Morex and TM194 mutant using force spectroscopy under plasmolysed but hydrated conditions (33, 34). Specifically, we characterised 9 independent areas within the elongation zone in a 3 x 3 array (Fig. S19a), performing $100 < n < 360$ indentation curves for each biological replicate (Morex = 4 and TM194 = 5). The obtained force versus distance curves were used to determine apparent stiffness (pN/nm) (Fig. S19b). Morex roots exhibited an average stiffness of 7.60 ± 3.30 pN/nm, while TM194 showed 5.6 ± 3.60 pN/nm (Fig. 4g). Our results suggest that there is a significant reduction (26.32%, *P*-value < 0.001) in cell wall stiffness in elongating cells of the *Hvegt1* mutant compared to wildtype. Interestingly, when sub-dividing analysed 3x3 array data into scored stele versus cortical tissues, mutant roots have a significantly lower stiffness in root cortical tissues (35.75%, P-value < 0.001), while there was no significant difference for stele tissues (Fig. S19c). Hence, reduced cell wall stiffness (notably in the cortical layers) in *hvegt1* mutant roots is likely to disrupt their ability to counteract gravitropic bending, causing them to grow steeper along a gravity vector.

Discussion

Root angle is a key trait in crops to ensure efficient capture of soil resources such as water and nutrients. Although recent studies have identified major QTLs associated with seminal root angle by genome wide association studies based on phenotyping of different barley genomic populations (35, 36), knowledge about the underlying genes controlling root angle in barley remains limited. A limited number of root angle regulatory genes have been identified in other cereals including *DRO1* (1), *VLN2* (37), *PIN2* (38), *RMD* (3) and *CIPK15* (2). To address this knowledge gap, we characterised a chemically mutagenized population of the cv. Morex (12) for a steeper seminal root phenotype, where we identified the TM194 mutant which exhibited steeper growth angle not only for seminal roots but also for lateral and crown roots. Genetic and genomic approaches revealed that a mutation in the *EGT1* (*ENHANCED GRAVTROPISM 1*) gene is responsible for the steeper root angle phenotype.

HvEGT1 encodes a Tubby-like protein (TLP) which contains conserved C-terminal tubby and N-terminal F-box domains (39, 40). Tubby domain containing proteins are proposed to act as bipartite transcription regulator (41, 42), whereas F-box proteins facilitate protein ubiquitination by acting as bridges between specific substrates and the components of the SCF-type (Skp1-Cullin-F-box) or ECS-type (ElonginC-Cullin-SOCS-box) E3 ubiquitin ligase complexes (39, 43). Previous mutant studies in *Arabidopsis thaliana* have identified that Tubby like proteins AtTLP3 and AtTLP2 could play roles in regulation of ROS signaling and cell wall related genes, respectively (44, 45). Consistent with this, our transcriptome analysis identified that ROS homeostasis and cell wall modifying enzymes are deregulated in mutants compare to wildtype, suggesting that some of these genes may represent downstream targets of *HvEGT1*. Protein-protein interaction database analysis suggests EGT1 might regulate proteins involved in cell elongation and cell expansion by regulating cell wall modifying enzymes or cell wall material synthesis or transport (Fig. S20). Further work will be required to pinpoint whether these are direct or indirect regulatory target(s) of EGT1. Kirschner et al. (46) recently reported a barley mutant with a steeper root growth angle phenotype termed *ENHANCED GRAVITROPISM 2* (EGT2) whose wildtype gene encoded a STERILE ALPHA MOTIVE containing protein also deregulates cell wall related genes. Although *EGT1* and *EGT2* both function in auxin independent AGO mechanisms, they are expressed in distinct tissue types and target different set of cell wall genes. Additionally, no change in *EGT1* expression was observed in *Hvegt2 mutant* and vice-versa (Fig. S21). Hence, *EGT1* and *EGT2* could function in parallel AGO pathways to control root angle in barley and wheat.

How does *EGT1* control root angle? *EGT1* expression is detected in stele and cortical cells in the root meristem and elongation zones (Fig. 4c), which overlaps with cortical cell wall stiffness differences detected using AFM in wildtype versus *Hvegt1* mutant root tips (Fig. S19). Interestingly, *Hvegt1* mutant root tips also show a reduction in ROS levels where *EGT1* is normally expressed (Fig. S13). ROS triggers cell wall cross-linking and increases stiffness (47). It is plausible that EGT1 functions to regulate ROS homeostasis in cortical tissues to control optimal stiffness required for maintaining roots at specific gravitropic set point angles. EGT1-dependent stiffening of cortical cell walls may serve to counteract the gravitropic machinery's known ability to bend roots via the outermost epidermal tissues (32). However, in the absence of EGT1, cell walls of root cortical tissues are less rigid, enabling the gravitropic machinery to bend the *Hvegt1* mutant root much more rapidly. Hence, we propose that auxin-dependent gravitropic bending operates in outer epidermal tissues, while auxin-independent EGT1 mediated stiffening mechanisms operate in root cortical tissues. Such a dual auxin-dependent/independent mechanical model for regulating root gravitropic bending rate also provides a simple mechanism for explaining gravitropic set point angle, where the relative strength of the auxin-dependent gravitropic and EGT1-dependent anti-gravitropic pathways operating in outer tissues (epidermis and cortex, respectively) could determine set point angle in different root classes.

Could new crop varieties with altered root angle be selected using *EGT1*? Loss of function *EGT1* alleles exhibit very steep angles for all root classes, likely causing them to inefficiently compete with each other for resource capture. However, results from haplotype analysis appear more promising since nucleotide polymorphisms within the *HvEGT1* sequence were observed to determine natural variation in root growth angle in a barley diversity panel. Hence, selecting or engineering *HvEGT1* alleles to adapt cultivars for specific environmental conditions such as different soil types or variable water table depth would appear possible. Further studies targeting EGT1 promise to open novel avenues for developing bespoke crop varieties with optimised root system architecture for efficient resource capture.

Materials and Methods

Plant Material

Barley *Hvegt1* mutant alleles (TM194 and TM3580, from the TILLMore barley mutant population (48), wheat *Tdegt1* mutant alleles (*Tdegt1_wtA/mutB, Tdegt1_mutA/wtB and Tdegt1_mutA/mutB,* from a wheat TILLING population described in (49) and respective wildtypes (cv. Morex and cv. Kronos) were used for root growth angle imaging and measurement analyses on flat screens using semi-hydroponic systems and in soil using rhizotrons and X-ray micro-computed tomography (microCT) and X-ray computed tomography (CT). An F_2 population obtained by crossing TM194 mutant and another barley wildtype cv. Barke was used for Bulk Segregant Analysis (BSA). TM194 and TM3580 mutant alleles were used for whole genome sequencing (WGS) experiment and mapped to Morex v.1 reference genome. Morex and *HvEGT1* mutant alleles (TM194 and TM3580) were used for RNAseq analysis and their WT and mutated protein sequences, respectively, were used for protein structure analysis. Morex and TM194 mutant were used for gravistimulus induced root bending assays (on mock, NAA and NPA supplemented media), Lugol's iodide staining, H_2DCFDA ROS detection assay and Atomic Force Microscope Spectroscopy experiments. Selected lines from the barley WHEALBI diversity panel (https://www.whealbi.eu/) were used for haplotype network analysis and root growth angle measurements. Methodology and growth conditions for each experiment are described below.

Barley and Wheat 2D root phenotyping

For semi-hydroponic system, seeds were washed in 70% ethanol for 1 min, then in 1% sodium hypochlorite + 0.02% TritonX-100 for 5 min and rinsed with distilled water. Sterilised seeds were pre-germinated for 24 h at 28 °C in wet filter paper. Equally germinated seeds were placed between two sheets of 50 x 25 cm of filter paper (Carta filtro Labor, Gruppo Cordenons SpA, Milan, Italy) soaked in demineralized water, rolled, positioned vertically in a 5-litres plastic beaker with 1 liter of demineralized water. Barley seedlings were grown for ten days at 24°C and wheat seedlings were grown for seven days at 22ºC with a 16/8 hours photoperiod. Root growth from both experiments were imaged using DSLR camera and vertical root angle for seminal and lateral (from the insertion with the seminal root) roots were calculated using ImageJ software. *For 2D soil experiment purpose*, barley and wheat *egt1* mutants and their respective wildtypes were grown up to 20 days in the GrowScreen-Rhizo rhizotrons automated platform and analysed as previously described (50).

Shoot and leaf growth angle measurements

For shoot growth angle measurements, plants of TM194 and Morex were grown in blue papers for 7 DAG with a day temperature of 21°C (16 h) and a night temperature of 18°C (8 h). Leaf growth angles were measured using the angle tool in FIJI. *N*=8 plants per genotype were used. *For leaf growth angle measurements*, plants of TM194 and Morex were grown in the greenhouse, in a peat and vermiculite growing medium (Vigorplant Irish and Baltic peat-based professional mix) in 15 × 15 × 30 cm polyethylene pots with a day temperature of 22°C (16 h) and a night temperature of 18°C (8 h). Greenhouse lighting was a mix of natural light supplemented with artificial light by 400-watt high-pressure sodium lamps (Sylvania SHP-TS 400W Grolux). Leaf growth angles were measured for the first three leaves of each plant, including the flag leaf, at flowering time (Zadoks growth stage 6). A goniometer was used to measure the angle between the proximal region of the adaxial surface of the blade and the stem.

Barley non-destructive 3D root phenotyping

Non-destructive 3D phenotyping was performed on Morex and TM194 using X-ray microCT and X-ray CT (n=6 independent replicates). *For X-ray microCT*, seeds were pre-germinated in petri dishes for 1 day at 21°C in dark. Successful seedlings with equally germinated roots were grown in PVC columns (8 cm diameter x 15 cm height) filled with sandy loam soil from UoN experimental farm field sieved at <2mm and maintained at notional field capacity moisture until 9 DAG. Each column was scanned using a Phoenix v|tome|x M ® 240kV X-ray microCT scanner (Waygate Technologies (a Baker Hughes business), Wunstorf, Germany) at the Hounsfield Facility (University of Nottingham, Sutton Bonington Campus, UK). The voltage and current were set at 180 kV and 180 µA, respectively. A voxel resolution of 55 µm was used in all scans. During the scan, the specimen stage rotated through 360º at a rotation step increment of 0.166º collecting a total of 2160 projection images. Each image was the integration of 4 frames with a detector exposure time of 250 ms, resulting in a 75 minutes scan time. A 0.1 mm copper filter was applied to the front of the exit window of the X-ray tube during the scan to reduce beam hardening artefacts. *For the X-ray CT*, well-watered plants were grown in larger PVC soil columns (20 cm diameter, 100 cm height) until full maturation stage. Each column was then scanned using a Phoenix v|tome|x L Custom ® 320kV X-ray CT system (Waygate Technologies (a Baker Hughes business), Wunstorf, Germany) at the Hounsfield Facility (University of Nottingham, Sutton Bonington Campus, UK). The voltage and current were set at 290 kV and 6200 µA respectively. A voxel resolution of 150 µm was used in all scans. During the scan, the specimen stage rotated through 360º at a rotation step increment of 0.15º collecting a total of 2400 projection images. To reduce image noise, each projection image was an integration of 12 frames with a detector exposure time of 131 ms. Each scan took approximately 240 minutes. A 1mm copper filter was applied to the exit window of the X-ray tube and a further 0.5mm Cu filter applied over the detector panel to reduce beam hardening artefacts.

For all CT images, the scans were reconstructed using DatosRec software (Waygate Technologies (a Baker Hughes business), Baker Hughes Digital Solutions GmbH, Wunstorf, Germany). Radiographs were visually assessed for sample movement before being reconstructed in 16-bit depth volumes with a beam hardening correction of 8. An inline median filter was applied to reduce noise in the image of the CT X-ray data. Reconstructed volumes were then post-processed in VGStudioMAX (version 2.2.0; Volume Graphics GmbH, Heidelberg, Germany). Root system architecture was first segmented from the reconstructed volumes using the polyline tool within VGStudioMAX and then quantified using an in-house software tool called PAM (Polyline Angle Measurement). PAM extracts the 3D coordinate points (2-5 XY slices apart) for each polyline and translates these into a 3D model. The angle of each polyline (root) is calculated from the difference of a vertical vector from the position of the uppermost coordinate point of the polyline (e.g., the soil surface). Therefore, steeply growing roots have a low angle value and shallow roots have a large angle value. Measurement of root angle was terminated once the root has touched or interacted with the pot wall to avoid any physical interference on undisturbed root angle.

Bulked segregant analysis (BSA)

BSA was carried out on F_2 plants derived from the cross TM194 $\times$ cv. Barke which were grown in flat rhizotrons, each composed by a rigid 38.5 x 42.5 cm black plastic screen and by two wet filter paper sheets. Seeds were disinfected for 5 minutes in a 1.2% solution of sodium hypochlorite and incubated for 24 hours at 28°C. Five pregerminated seeds per rhizotron were placed between two filter paper sheets. Rhizotrons were vertically positioned inside a plastic tank filled with deionized water to reach a level of 5 cm from the bottom and put in a growth chamber with a 16/8h photoperiod and a temperature of 22°/18°C for 13 days. After that period, root growth angles were measured, and seedlings were divided into wildtype and mutant phenotype groups. 15 plants from each group were selected for single plant DNA extraction. Leaves were lyophilized and foliar samples of approximately 2 cm^2 were homogenized for 3 minutes in a TissueLyser. DNA was extracted with the Macherey-Nagel Nucleospin® Plant II kit and quantified with NanoDrop. Two DNA bulks, steeper and wildtype root angle phenotype were prepared in double, mixing equal amounts of each plant and bringing to a final concentration of 50 ng/ul, in addition to single plant DNA from 10 plants showing steeper angle and all sample were genotyped with the 9k Illumina Infinium iSelect barley SNP array. The results were analysed with GenomeStudio (Illumina, San Diego, Inc.), and delta theta values used as index of allele proportion at each SNP marker. Delta theta values were calculated as the squared difference between the theta value of wildtype and steeper angle phenotype bulk.

Whole genome sequencing (WGS)

Genomic DNA for WGS of the two mutants TM194 and TM3580 was prepared as described above and sequenced with Illumina HiSeq PE150, obtaining 727,190,417 paired-end reads for an average coverage of approximately 23x for TM194 and 792,713,857 paired-end reads for an average coverage of approximately 25x for TM3580. Reads were aligned to Morex v.1 reference sequence (51) with BWA v.7.12 (52) and variants in the genomic space were called with SAMtools v.1.3(53), filtering for a minimum read depth of 5x, PHRED quality > 40. To discard background mutations due to the differences between the Morex reference sequence and the Morex parental seeds which had previously been used in the mutagenesis, the SNP calling for TM194 considered further eight TILLMore mutants WGS data that was available at that moment, filtering with a custom AWK script for a minimum ratio DV/DP of 0.8 for the *Hvegt1* mutants and a maximum ratio of 0.2 in every other mutant, where DP is the coverage depth at the SNP position and DV is number of non-reference bases at the same position. SNP effects were predicted with SNPEff v.3.0.7 (54). TM194 mutant was predicted to harbour a mis-sense substitution within 4^{th} exon while TM3580 mutation at the end of first intron was predicted to cause splice-acceptor variant (SI Dataset 1).

Haplotype analysis of *HvEGT1* in WHEALBI barley germplasm collection

A haplotype analysis of SNP data from the barley diversity panel WHEALBI (55), consisting of 459 barley accessions, of which 199 are cultivars, 202 landraces and 4 wild, was conducted in the coding region of *HvEGT1*. Files were imported into R Studio and package *pegas* (56) v.0.14 was used to detect haplotypes. Six haplotypes were found. The MUSCLE multi-alignment was produced with Mega X v.10.2.4 (57) and exported to the NEXUS format (58). The haplotype TCS network (59) was produced with PopART (http://popart.otago.ac.nz).

HVEGT1 structure modelling and *Hvegt1* mutant allele mapping

The protein sequence obtained by translating Transcript 3 (427 aa) from *HvEGT1* (*HORVU6Hr1G068970*) entry was used to construct a homology model using the Phyre2 (60) server. A homology modelling approach was chosen over *de novo* structure prediction from first principles as the gene of interest was inferred to have F-box and Tubby-Like domains, which were confirmed by the protein domain analysis using EBI Interproscan tool. Tubby-Like domain was alone used in the structure prediction algorithm. WGS and haplotype analysis identified mis-sense amino acid substitutions (TM194 and Haplotype II and IV, respectively) were mapped on the predicted structure. Splice acceptor mutation (TM3580) was also visualised with respect to organised F-box and Tubby-like domains. Protein sequence was further studied for its conservation to function prediction across plant species using ConSurf algorithm.

Wheat EGT1 mutant identification

Durum wheat (*Triticum turgidum*) *Tdegt1* mutants were identified from a TILLING population developed in tetraploid *cv* Kronos (49). Two selected lines (Kronos2551 and Kronos3926) carrying premature termination codons in TRITD6Bv1G159700, the *TdEGT1* homoeologous gene on the B genome (*TdEGT1_wtA/mutB*), were both crossed with the line Kronos2708, carrying a splice donor mutation in TRITD6Av1G172130, the *TdEGT1* homoeologous gene on the A genome (*TdEGT1_mutA/wtB*). F1 plants obtained from both crosses were self-pollinated. Progenies of selected wild-type, single and double mutant F2 individuals derived from the two independent initial crosses (*TdEGT1_mutA/mutB*) were grown in semi-hydroponic system and analysed for seminal root angle analysis as mentioned above.

Phylogenetic analysis of Tubby-like F-Box Protein Sequences in selected monocots

HvEGT1 was used as a seed gene to select orthologous genes (>40% identity) from key monocot species such as barley (*Hordeum Vulgare*), wheat (*Triticum turgidum*), rice (*Oryza Sativa spp. Japonica*), maize (Zea Mays B73) and brachypodium (*Brachypodium distachyon*) using interactive phylogenetic module of Monocots Plaza 4.5 (61). Protein sequences were aligned using MUSCLE and tree was constructed using FastTree algorithm. Generated Newick file was imported into iTOL to create an unrooted tree.

Lugol's staining assay

To visualise statoliths in root tips of Morex and TM194 mutant, 1 day pregerminated seedlings were grown in paper rolls in 21 ºC, 16/8 daylight photoperiod growth conditions for 5 days. 1 cm root tips were then embebed in 10% low melting point agarose and sliced using vibratome (7000 smz-2, Campden Instruments, UK) set as 5 0Hz frequency, 1 mm amplitude and 40 µm section. Sections were stained using Lugol's iodine solution (VWR chemicals) for 3 minutes and then visualised using LEICA DM 550B light microscope.

Gravity and auxin sensitivity bioassays

Seedlings of Morex and TM194 mutant were pre-germinated for 2 days in dark at 21ºC. Equally germinated seeds were then transferred on 12cm squared plates containing 1% agar media and grown 1-2 days at 21ºC with 12/12 hours photoperiod. For gravity response bending bioassay, plates were then rotated by 30º, 60º and 90º and then images were collected at multiple timepoints using a Nikon D5100 camera. For the auxin sensitivity assay, seedlings were then transferred to mock, 10nM NAA and 1µM NPA media for 2 hours before rotating plates by 90º. Time lapse image stack was then generated by taking images every 30 minutes for 12 hours in dark and then once at 24 hours after gravistimulus using the robotic imaging facility at the University of Nottingham. Root tip bending angle was the quantified using FIJI (62).

RNA-sequencing and data analysis

Seeds of Morex, TM194, TM3580 genotypes were sterilised with 0.5% Sodium hypochlorite solution for 5 mins followed by five washes of sterile water. Sterilised seeds were germinated on sterile Whatman filter paper placed in a petri dish for 2 days at 21ºC in dark. Equally germinated seeds were vertically grown on 1% agar plates for 2 days at 22ºC, 16/8 hours photoperiod. Root tips from seminal roots growing on media surface were dissected at the first visible root hairs and samples were snap frozen using liquid nitrogen and then stored at -80ºC. Root tips from 15 seedlings were pooled together per replicate and RNA extraction was then performed using Trizol and Rneasy mini kit (Qiagen) for RNA seq analysis. For each genotype, 4 biological replicates were prepared.

Library preparation and Illumina sequencing was performed by Novogene (UK) Company Limited. RNAseq was performed on an Illumina Hiseq 2000 platform and 150 bp paired end reads were generated according to Illumina's protocol. Data analysis was performed by standard Novogene bioinformatics pipeline. Raw reads were first processed to remove adapter and poly-N sequences and low-quality reads. High quality paired-end clean reads were mapped to reference genome IBSC_v2 using HISAT2 (63) software. Cufflinks Reference Annotation Based Transcript (RABT) assembly method (64) was used to assemble the set of transcript isoforms of each bam file obtained din the mapping step. HTSeq (65) was used to count the read numbers mapped of each gene, including known and novel genes. FPKM of each gene was calculated based on the length of the gene and reads counts mapped to this gene. The hierarchical cluster analysis of gene expression among replicates indicated poor correlation for one of the four replicates for sample TM194, which was removed from further analysis. Differential expression analysis between TM194 vs Morex, TM3580 vs Morex and TM3580 vs TM194 was performed using DESeq2 (66) R package. The resulting *P* values were FDR corrected using the Benjamini and Hochberg's approach and genes with an adjusted *P* value < 0.05, -1.5 < fold change > 1.5 and FPKM >1 were assigned as differentially expressed. GO enrichment was performed using gProfiler (67) web server with settings (Statistical domain space = All known genes; significance threshold = g:SCS, 0.05). REVIGO (68) (http://revigo.irb.hr, default settings) was used to remove semantically redundant GO terms.

ROS detection assay

TM194 mutant and Morex seeds were surface sterilised using 20% (v/v) bleach for 4 minutes and were then rinsed five times with de-ionised water. Washed seeds were then germinated on a filter paper saturated with de-ionised water in a petri dish kept at 21 ºC for 48 hours. Seedlings with uniform growth were placed on a germination paper, rolled into paper rolls and grown vertically at 21 ºC for 4 days. CM-H_2DCFDA (Sigma-Aldrich) dissolved into dimethyl sulfoxide (DMSO, VWR Life Science) was used to visualize the localization of ROS in Morex and TM194 mutant root tips. 20 µM CM-H_2DCFDA was prepared in 50 µM potassium chloride buffer (50mM KCl, 10mM MES, pH 6.0) on the day of the experiment. Root samples were taken 1 cm from the tip and were treated with 1 ml of CM-H2DCFDA for 15 minutes under vacuum. After treatment, samples were washed thoroughly with potassium chloride buffer four times. Samples were then placed on a

glass slide with 50% glycerol as mounting agent and visualized with the Zeiss Leica DM5000 fluorescent microscope. CM-H_2DCFDA could be deacetylated by cellular esterase and then subject to oxidisation by ROS to 2',7'-dichlorofluorescein (DCF), which is highly fluorescent and could be detected under excitation and emission spectra of 492-495 nm and 517-527 mm, respectively. To minimize any variation in processing and imaging samples, all roots per seedling were stained, mounted on one glass slide and imaged together. Gain was adjusted for each slide at the saturation limit of the root showing maximum glow and then set for all the roots on the same slide. To identify any spatial differences in ROS accumulation in each root, we took multiple high magnification fluorescent images along the longitudinal axis of root and stitched them into one complete image. This stitched image was then quantified in five different developmental zones: 4 equal length zones between root tip and first visible root hair and the last one as root hair differentiation zone. Mean fluorescent value for each zone was calculated in FIJI. Two biological replicates were performed with 4 seedlings per replicate and 4-5 seminal root tips per seedling were analysed. Statistical analysis was performed using Welch's t-test in "RStudio". *, **, *** indicate significant P-value < 0.05, 0.01, 0.001 (n roots=16-20 , n plants=4 , n= 2 experiments).

Barley RNA *in situ* hybridisation

RNA *in situ* hybridization was performed to target *HvEGT1* expression in Morex. Seeds of barley cultivar Morex were surface sterilized in 20% (v/v) sodium hypochlorite solution for 10 min, then rinsed with MilliQ water five times before pre-germination overnight. Seeds were then placed into germination pouches (Phytotc) for 5 days. Fresh root tips (2 cm) were harvested and fixed in Formalin-Acetic acid-Alcohol (FAA) (50%v/v 100% ethanol, 5%v/v glacial acetic acid, 25%v/v 16% paraformaldehyde (electron microscopy grade), 20%v/v diethyl pyrocarbonate (DEPC)-H_2O, 0.1%v/v Tween 20). Root tips with FAA were placed on ice for 2 hours including 15 min of vacuum infiltration, followed by two 10 min washes in 70% ethanol/DEPC-H_2O, and then stored at 4°C overnight. The samples were dehydrated and cleared with a series of ethanol and Histochoice washes before being embedded in molten paraffin wax. The embedded samples were stored at 4°C under Rnase free conditions before sectioning. The paraffin wax blocks with the root samples were sectioned at 7 µm thickness using a Leica microtome and mounted onto poly-L-lysine coated slides prior to in situ hybridization. Digoxigenin-labeled antisense and sense probes were designed and synthesized as shown in Fig. S10. The probes specific to *HvEGT1* were amplified from Morex root cDNA, using primers fused with the T7 promoter sequence at the 5' end to allow in vitro transcription. The probes were designed to recognize the end of the coding sequence and 3' untranslated region (UTR) of the gene. The barley histone H4 gene was used as a positive control. The *in-Situ* hybridization and detection were performed using the InsituPro Vsi robot (Intavis) (69).

Force spectroscopy using Atomic Force Microscope

Sample preparation: Root tips from 4-day old seedlings of Morex and TM194 were grown in 1 % agar (Scientific Laboratory Supplies) at 23ºC, 16/8h daylight/darkness. Root tips from seminal roots were harvested at 1.5 cm, set in 5 % agarose (Sigma-Aldrich, UK) creating 2 cm x 1 cm blocks for cross sectioning. Longitudinal cross-sections of 50 µm were obtained using a vibratome (Frequency 50 Hz, Amplitude 1mm) (7000smz-2, Campden Instruments, UK) and observed using light microscopy to confirm stele and cortical tissues were correctly exposed with visible elongation zone. Specimens were then stored in de-ionised water at 4ºC overnight and analysed by Atomic Force Microscope (AFM) one day after preparation. *Atomic Force Microscopy* Mechanical Analysis: A Dimension ICON (Bruker Nano, Santa Barbara, CA, USA) using dedicated software (Nanoscope 9.4) was used probe all root samples. MLCT-E (Bruker Nano, Santa Barbara, CA) cantilevers were used across all analysed samples. Before mounting the MLCT-E cantilever, all other cantilevers on the same AFM probe were removed using fine tweezers guided by a binocular. This was performed to avoid parallel probes causing localised

sample surface movement interfering with the indentation measurements. AFM probes were then mounted and secured to a fluid cell (DECAFMCH-PFT, Bruker Nano, Santa Barbara, CA, USA) and calibrated in de-ionised water before analysis. The average spring constant of cantilevers used in experiments was 0.008 ± 0.002 N/m. Root sections in agarose were fixed to glass slides using UHU Plus 2 min curing glue (Bolton Adhesives, NL) on the exterior of agarose only and hydrated using de-ionised water for 30 mins before AFM analysis. Operating in force-spectroscopy mode under water hydrated conditions, 9 independent areas were monitored within the observable elongation zone in a 3 x 3 array shown in Fig. S19a. Indentations were performed in the observable centre of root meristem cells on each section generating a total of 100 < n < 360 force curves for each biological replicate (Morex = 4, TM194 = 5). Using dedicated software (Nanoscope Analysis 1.9), apparent stiffness (pN/nm) values were obtained from individual force-distance curves using a contact point based fit and linear stiffness model. Data from each area was pooled and analysed using a non-parametric Wilcoxon test for significant differences between sample type and areas ($p < 0.001$). Additionally, data from these 9 areas were categorized into cortical and stele tissues and the results of comparison between Morex and TM194 are shown in Fig. S19c.

qPCR analysis during NAA and NPA treatments

Morex and egt1 mutant TM194 seeds were sterilized with 70% ethanol for 5 mins then 15% bleach for 5 min and washed 3-5 times with distilled water. Sterilised seeds were sown directly on ½ Hoagland's No. 2 Basal salt (Sigma, H2395), 1% agar plates and plates were kept at 4ºC for 5 days to improve germination rate. Plates were then transferred to growth room with 16/8h photoperiod and temperature of 22°/18°C. 3-day old plants (post germination) were then transferred to plates containing ½ Hoagland's solution, 1% agar, 0.1% DMSO, plus either 10nM NAA or 1µM NPA. Root tips (5mm form tip) from > 3 individual plants (i.e., ~15 plants) were pooled at 0h and 8h post transfer and flash frozen in liquid nitrogen. RNA was extracted using the Monarch® Total RNA Miniprep Kit (NEB, T2010S) as per protocol and cDNA prepared using Thermo Scientific Revertair frist strand cDNA synthesis kit. Quantitative RT-PCR (qRT-PCR) analysis was carried out with SYBRgreen (Meridian bioscience, Sensimix SYBR Hi-ROX Kit) using qTower 384G machine (Analytikjena). *HvAlpha-Tub* (*HORVU1Hr1G081280.1*) and *HvGADPH* (*HORVU6Hr1G054520*) were used as internal control, for primers see Supplementary Table 1. Three independent biological repeats with four technical replicates were used. Data was analysed using delta Ct method and statistical analysis carried out using Student's *T*-test. Each treated sample per genotype was normalised by respective DMSO sample.

Acknowledgments

We acknowledge the technical support of Simona Corneti, Anne Fiebig, Sandra Stefanelli, Alessandro Tondelli. RF acknowledges ARPA-E DEEPER (USDOE ARPA-E ROOTS Award Number DE-AR0000821) and the Hounsfield Facility Center at the University of Nottingham for all the support provided for this work. The Hounsfield Facility received funding from European Research Council (Futureroots Project, Grant agreement ID: 294729), Biotechnology and Biological Sciences Research Council of the United Kingdom and The Wolfson Foundation. RaB thanks Future Food Beacon Nottingham Research and BBSRC Discovery Fellowship (BB/S011102/1). The rhizotron study received funding from the European Union's Horizon 2020 research and innovation programme under grant agreement No 731013 (EPPN2020). Work described here is supported in part by the project 'Rooty- A root ideotype toolbox to support improved wheat yields' funded by the IWYP Consortium (project IWYP122) via the Biotechnology and Biological Sciences Research Council in the United Kingdom (BB/S012826/1). HL was supported by a joint University of Adelaide - University of Nottingham PhD scholarship. ANB acknowledges Anne McLaren Fellowship at University of Nottingham. B.K.P acknowledge challenge grant (CHG\R1\170040) and BBSRC Discovery Fellowship (BB/V00557X/1). GEY acknowledges the financial support from the Biotechnology and Biological Sciences Research

Council grant (BB/T006404/1). We acknowledge Francesco Loreto (CNR-DISBA, Italy) for supporting M.L.'s visit to Nottingham.

References

1. Y. Uga, *et al.*, Control of root system architecture by DEEPER ROOTING 1 increases rice yield under drought conditions. *Nat Genet* **45**, 1097–1102 (2013).
2. H. M. Schneider, *et al.*, Root angle in maize influences nitrogen capture and is regulated by calcineurin B-like protein (CBL)-interacting serine/threonine-protein kinase 15 (ZmCIPK15). *Plant Cell Environ* **45**, 837–853 (2022).
3. G. Huang, *et al.*, Rice actin binding protein RMD controls crown root angle in response to external phosphate. *Nat Commun* **9**, 2346 (2018).
4. Y. Kitomi, *et al.*, Root angle modifications by the DRO1 homolog improve rice yields in saline paddy fields. *Proc National Acad Sci* **117**, 21242–21250 (2020).
5. S. Roychoudhry, M. Del Bianco, M. Kieffer, S. Kepinski, Auxin Controls Gravitropic Setpoint Angle in Higher Plant Lateral Branches. *Curr Biol* **23**, 1497–1504 (2013).
6. S. Roychoudhry, *et al.*, The developmental and environmental regulation of gravitropic setpoint angle in Arabidopsis and bean. *Sci Rep-uk* **7**, 42664 (2017).
7. I. Ottenschläger, *et al.*, Gravity-regulated differential auxin transport from columella to lateral root cap cells. *Proc National Acad Sci* **100**, 2987–2991 (2003).
8. R. Swarup, *et al.*, Root gravitropism requires lateral root cap and epidermal cells for transport and response to a mobile auxin signal. *Nat Cell Biol* **7**, 1057–1065 (2005).
9. L. R. Band, *et al.*, Root gravitropism is regulated by a transient lateral auxin gradient controlled by a tipping-point mechanism. *Proc National Acad Sci* **109**, 4668–4673 (2012).
10. M. R. Rosquete, *et al.*, An Auxin Transport Mechanism Restricts Positive Orthogravitropism in Lateral Roots. *Curr Biol* **23**, 817–822 (2013).
11. S. Roychoudhry, M. Del Bianco, M. Kieffer, S. Kepinski, Auxin Controls Gravitropic Setpoint Angle in Higher Plant Lateral Branches. *Curr Biol* **23**, 1497–1504 (2013).
12. V. Talamè, *et al.*, TILLMore, a resource for the discovery of chemically induced mutants in barley. *Plant Biotechnol J* **6**, 477–485 (2008).
13. S. Mairhofer, C. J. Sturrock, M. J. Bennett, S. J. Mooney, T. P. Pridmore, Extracting multiple interacting root systems using X-ray microcomputed tomography. *Plant J* **84**, 1034–1043 (2015).
14. D. Bustos-Korts, *et al.*, Exome sequences and multi-environment field trials elucidate the genetic basis of adaptation in barley. *Plant J* **99**, 1172–1191 (2019).
15. L. A. Kelley, S. Mezulis, C. M. Yates, M. N. Wass, M. J. E. Sternberg, The Phyre2 web portal for protein modeling, prediction and analysis. *Nat Protoc* **10**, 845–858 (2015).
16. J. Jumper, *et al.*, Highly accurate protein structure prediction with AlphaFold. *Nature* **596**, 583–589 (2021).
17. K. V. Krasileva, *et al.*, Uncovering hidden variation in polyploid wheat. *Proc National Acad Sci* **114**, E913–E921 (2017).
18. S. Roychoudhry, *et al.*, The developmental and environmental regulation of gravitropic setpoint angle in Arabidopsis and bean. *Sci Rep-uk* **7**, 42664 (2017).
19. J. Friml, J. Wiśniewska, E. Benková, K. Mendgen, K. Palme, Lateral relocation of auxin efflux regulator PIN3 mediates tropism in Arabidopsis. *Nature* **415**, 806–809 (2002).
20. R. Swarup, *et al.*, Root gravitropism requires lateral root cap and epidermal cells for transport and response to a mobile auxin signal. *Nat Cell Biol* **7**, 1057–1065 (2005).
21. L. R. Band, *et al.*, Root gravitropism is regulated by a transient lateral auxin gradient controlled by a tipping-point mechanism. *Proc National Acad Sci* **109**, 4668–4673 (2012).
22. M. R. Rosquete, *et al.*, An Auxin Transport Mechanism Restricts Positive Orthogravitropism in Lateral Roots. *Curr Biol* **23**, 817–822 (2013).

23. Q. Shi, *et al.*, Genome-wide characterization and expression analyses of the auxin/indole-3-acetic acid (Aux/IAA) gene family in barley (Hordeum vulgare L.). *Sci Rep-uk* **10**, 10242 (2020).
24. F. Tian, D.-C. Yang, Y.-Q. Meng, J. Jin, G. Gao, PlantRegMap: charting functional regulatory maps in plants. *Nucleic Acids Res* **48**, D1104–D1113 (2019).
25. J. Shigeto, Y. Tsutsumi, Diverse functions and reactions of class III peroxidases. *New Phytol* **209**, 1395–1402 (2016).
26. M. R. Tucker, *et al.*, Exploring the Role of Cell Wall-Related Genes and Polysaccharides during Plant Development. *Plants* **7**, 42 (2018).
27. R. A. Burton, M. J. Gidley, G. B. Fincher, Heterogeneity in the chemistry, structure and function of plant cell walls. *Nat Chem Biol* **6**, 724–732 (2010).
28. K. F. X. Mayer, *et al.*, A physical, genetic and functional sequence assembly of the barley genome. *Nature* **491**, 711–716 (2012).
29. H. Takehisa, *et al.*, Genome-wide transcriptome dissection of the rice root system: implications for developmental and physiological functions. *Plant J* **69**, 126–140 (2012).
30. Y. Sato, *et al.*, RiceXPro Version 3.0: expanding the informatics resource for rice transcriptome. *Nucleic Acids Res* **41**, D1206–D1213 (2013).
31. J. Zeng, Z. Dong, H. Wu, Z. Tian, Z. Zhao, Redox regulation of plant stem cell fate. *Embo J* **36**, 2844–2855 (2017).
32. R. J. Dyson, *et al.*, Mechanical modelling quantifies the functional importance of outer tissue layers during root elongation and bending. *New Phytologist* **202**, 1212–1222 (2014).
33. S. A. Braybrook, A. Peaucelle, Mechano-Chemical Aspects of Organ Formation in Arabidopsis thaliana: The Relationship between Auxin and Pectin. *Plos One* **8**, e57813 (2013).
34. A. Peaucelle, *et al.*, Pectin-Induced Changes in Cell Wall Mechanics Underlie Organ Initiation in Arabidopsis. *Curr Biol* **21**, 1720–1726 (2011).
35. Z. Jia, *et al.*, Genetic Dissection of Root System Architectural Traits in Spring Barley. *Front Plant Sci* **10**, 400 (2019).
36. H. Robinson, *et al.*, Genomic Regions Influencing Seminal Root Traits in Barley. *Plant Genome* **9**, 0 (2016).
37. S. Wu, *et al.*, VLN2 Regulates Plant Architecture by Affecting Microfilament Dynamics and Polar Auxin Transport in Rice. *Plant Cell* **27**, 2829–2845 (2015).
38. L. Wang, *et al.*, LARGE ROOT ANGLE1, encoding OsPIN2, is involved in root system architecture in rice. *J Exp Bot* **69**, 385–397 (2017).
39. J. M. Gagne, B. P. Downes, S.-H. Shiu, A. M. Durski, R. D. Vierstra, The F-box subunit of the SCF E3 complex is encoded by a diverse superfamily of genes in Arabidopsis. *Proc National Acad Sci* **99**, 11519–11524 (2002).
40. C.-P. Lai, *et al.*, Molecular Analyses of the Arabidopsis TUBBY-Like Protein Gene Family. *Plant Physiol* **134**, 1586–1597 (2004).
41. T. J. Boggon, W.-S. Shan, S. Santagata, S. C. Myers, L. Shapiro, Implication of Tubby Proteins as Transcription Factors by Structure-Based Functional Analysis. *Science* **286**, 2119–2125 (1999).
42. S. Santagata, *et al.*, G-Protein Signaling Through Tubby Proteins. *Science* **292**, 2041–2050 (2001).
43. B. T. Kile, *et al.*, The SOCS box: a tale of destruction and degradation. *Trends Biochem Sci* **27**, 235–241 (2002).
44. M. U. Reitz, *et al.*, The Subcellular Localization of Tubby-Like Proteins and Participation in Stress Signaling and Root Colonization by the Mutualist Piriformospora indica. *Plant Physiol* **160**, 349–364 (2012).
45. M. Wang, *et al.*, Tubby-like Protein 2 regulates homogalacturonan biosynthesis in Arabidopsis seed coat mucilage. *Plant Mol Biol* **99**, 421–436 (2019).
46. G. K. Kirschner, *et al.*, ENHANCED GRAVITROPISM 2 encodes a STERILE ALPHA MOTIF–containing protein that controls root growth angle in barley and wheat. *P Natl Acad Sci Usa* **118**, e2101526118 (2021).

47. R. Schmidt, A. B. Kunkowska, J. H. M. Schippers, Role of Reactive Oxygen Species during Cell Expansion in Leaves. *Plant Physiol* **172**, 2098–2106 (2016).
48. V. Talamè, *et al.*, TILLMore, a resource for the discovery of chemically induced mutants in barley. *Plant Biotechnol J* **6**, 477–485 (2008).
49. K. V. Krasileva, *et al.*, Uncovering hidden variation in polyploid wheat. *Proc National Acad Sci* **114**, E913–E921 (2017).
50. K. A. Nagel, *et al.*, GROWSCREEN-Rhizo is a novel phenotyping robot enabling simultaneous measurements of root and shoot growth for plants grown in soil-filled rhizotrons. *Funct Plant Biol* **39**, 891–904 (2012).
51. M. Mascher, *et al.*, A chromosome conformation capture ordered sequence of the barley genome. *Nature* **544**, 427–433 (2017).
52. H. Li, R. Durbin, Fast and accurate short read alignment with Burrows–Wheeler transform. *Bioinformatics* **25**, 1754–1760 (2009).
53. H. Li, A statistical framework for SNP calling, mutation discovery, association mapping and population genetical parameter estimation from sequencing data. *Bioinformatics* **27**, 2987–2993 (2011).
54. P. Cingolani, *et al.*, A program for annotating and predicting the effects of single nucleotide polymorphisms, SnpEff. *Fly* **6**, 80–92 (2012).
55. W. Consortium, Single-nucleotide polymorphism matrices for 403 barley genotypes (WHEALBI diversity panel) (2019) https:/doi.org/10.5447/ipk/2019/5.
56. E. Paradis, pegas: an R package for population genetics with an integrated–modular approach. *Bioinformatics* **26**, 419–420 (2010).
57. S. Kumar, G. Stecher, M. Li, C. Knyaz, K. Tamura, MEGA X: Molecular Evolutionary Genetics Analysis across Computing Platforms. *Mol Biol Evol* **35**, 1547–1549 (2018).
58. D. R. Maddison, D. L. Swofford, W. P. Maddison, D. Cannatella, Nexus: An Extensible File Format for Systematic Information. *Systematic Biol* **46**, 590–621 (1997).
59. M. Clement, Q. Snell, P. Walke, D. Posada, K. Crandall, TCS: estimating gene genealogies. *Proc 16th Int Parallel Distributed Process Symposium*, 7 pp (2002).
60. L. A. Kelley, S. Mezulis, C. M. Yates, M. N. Wass, M. J. E. Sternberg, The Phyre2 web portal for protein modeling, prediction and analysis. *Nat Protoc* **10**, 845–858 (2015).
61. M. Van Bel, *et al.*, PLAZA 4.0: an integrative resource for functional, evolutionary and comparative plant genomics. *Nucleic Acids Res* **46**, gkx1002- (2017).
62. J. Schindelin, *et al.*, Fiji: an open-source platform for biological-image analysis. *Nat Methods* **9**, 676–682 (2012).
63. D. Kim, J. M. Paggi, C. Park, C. Bennett, S. L. Salzberg, Graph-based genome alignment and genotyping with HISAT2 and HISAT-genotype. *Nat Biotechnol* **37**, 907–915 (2019).
64. A. Roberts, H. Pimentel, C. Trapnell, L. Pachter, Identification of novel transcripts in annotated genomes using RNA-Seq. *Bioinformatics* **27**, 2325–2329 (2011).
65. S. Anders, P. T. Pyl, W. Huber, HTSeq—a Python framework to work with high-throughput sequencing data. *Bioinformatics* **31**, 166–169 (2015).
66. S. Anders, W. Huber, Differential expression analysis for sequence count data. *Nat Précéd*, 1–1 (2010).
67. U. Raudvere, *et al.*, g:Profiler: a web server for functional enrichment analysis and conversions of gene lists (2019 update). *Nucleic Acids Res* **47**, W191–W198 (2019).
68. F. Supek, M. Bošnjak, N. Škunca, T. Šmuc, REVIGO Summarizes and Visualizes Long Lists of Gene Ontology Terms. *Plos One* **6**, e21800 (2011).
69. J. Zeng, Z. Dong, H. Wu, Z. Tian, Z. Zhao, Redox regulation of plant stem cell fate. *Embo J* **36**, 2844–2855 (2017).
70. U. Raudvere, *et al.*, g:Profiler: a web server for functional enrichment analysis and conversions of gene lists (2019 update). *Nucleic Acids Res* **47**, W191–W198 (2019).
71. F. Supek, M. Bošnjak, N. Škunca, T. Šmuc, REVIGO Summarizes and Visualizes Long Lists of Gene Ontology Terms. *Plos One* **6**, e21800 (2011).

912 **Figure legends**

Fig. 1. TM194 mutant shows steeper angle in every root class in soil conditions

a, Representative X-Ray micro-CT scan image of 10 DAG wildtype (Morex) and TM194 roots, showing major differences in seminal root vertical angle. Scale bar = 2 cm. **b**, Representative X-Ray CT scan image of fully grown plants at grain maturation stage revealing major difference in crown root vertical angle between Morex and TM194. Scale bar = 10 cm. **c**, Representative image of 20 DAG Morex and TM194 revealing difference in lateral root insertion angles (red coloured). Scale bar = 10 cm **d**, Quantification of vertical root angle from segmented seminal roots, crown roots and lateral roots. *** and ** indicates statistically significant difference using Welch's *T*-Test at $p<0.001$ and $p<0.001$ in $n>4$ independent replicates, respectively. CT = computed tomography, DAG = days after germination.

913

914

915

Fig. 2. Exome and WGS sequencing of TM194 identifies mutation in *EGT1*

a-b, SNP based Bulk Segregant Analysis (BSA) from F2 plants from TM194 X cv. Barke outcross. **a**, Genome-wide plot of unbalanced allelic frequency from SNP-based BSA. △Theta parameter represents the difference in allele frequency for each tested SNP. **b**, Schematic representing a region spanning ~c.130 Mb on chromosome 6H between markers *BOPA2_12_30144* and *BOPA1_4109-90*. Filled circles indicate all SNPs within genes present in this region while empty circles (in red rectangle) indicate SNPs within pinpointed *HORVU6Hr1G068970* gene. Whole-Genome Shotgun (WGS) sequencing of another mutant allele of *HORVU6Hr1G068970* also showed steeper root growth angle phenotype. This gene is further named as *ENHANCED GRAVITROPISM 1* (*EGT1*). **c**, Schematic representation of *EGT1* and the position of the two mutations in relation to the F-box domain (red) and the Tubby-like protein domains. **d-e**, Haplotype analysis of *EGT1* nucleotide sequence variation present in WHEALBI barley germplasm collection. **d**, Haplotype network analysis revealed that haplotype II and IV carry missense substitutions, while remaining four haplotypes carry synonymous substitutions. *n* indicates number of genotypes within each class. **e**, Root growth angle distribution of WHEALBI barley lines carrying haplotype II (86 lines) and IV (25 lines).

916

917

Fig. 3. HvEGT1 controls root growth angle via auxin-independent anti-gravitropic offset (AGO) mechanism

a, Representative images of root bending response of 4-day old seminal roots in Morex and TM194 at 0.5, 1, 2 and 3 hours after 90º tilting gravistimulus. **b**, Measurement of dynamic change in root tip bending angle with increasing titling angle gravistimulations (from 30º to 60º to 90º) in Morex and TM194. **c-d**, Auxin root bending sensitivity assay. Quantification of root bending response in Morex and TM194 at 0.5, 3, 9,12 and 24 hours after a 90º gravistimulus during **a**, exogenous application of 10nM 1-Naphthaleneacetic acid (NAA) and **b**, 1µM auxin transport inhibitor 1-N-Napthylphthalamic acid (NPA). * represents statistically significant difference, between treated and mock samples from respective genotype, assessed using Welch's *T*-Test at $p<0.01$ in $n=2$ independent replicates.

Fig. 4. HvEGT1 transcriptionally regulates peroxidases and cell wall loosening enzymes and controls root cell wall stiffness

a, Pruned version of GO enrichment of genes differentially expressed between Morex and both *hvegt1* mutant alleles (-1.5<FC>1.5; Benjamini Hochberg FDR corrected Pvalue < 0.05; FPKM>=1). gProfiler (70) web server was used to perform GO enrichment analysis (settings: Statistical domain space = All known genes; significance threshold = g:SCS, 0.05) (SI Dataset 3). GO enrichments were pre-filtered using REVIGO (71) (http://revigo.irb.hr, default settings) to remove semantically redundant GO terms. Terms were pruned on REVIGO frequency (>0.25% and <2.5%) and top 5 most significant GO categories visualized. **b**, Schematic of gravitropic sensing and responding machinery in relation to root meristematic zones in barley cv. *Morex*: Maturation zone (MT), Elongation zone (EZ), Basal Meristem (BM), Quiescent Center (QC), Columella (CM), blue line identifies the transition zone, yellow arrows highlight the approximate region where the cross sections were taken (**d, e, f**) (scale bar=100µm). **c**, *In Situ* Hybridisation (ISH) on longitudinal section of root tips of cv. Morex with *HvEgt1* anti-sense probe. **d-f**, ISH of root tip cross-sections in cv. Morex with *HvEGT1* anti-sense probe in ED (**d**), higher PM (**e**) and lower PM (**f**) (scale bar=100µm). **g**, Force spectroscopy results showing stiffness values between Morex and TM194. *** indicates p value < 0.001 using non-parametric Wilcoxon test. **h**, Schematic of the proposed model. Auxin-dependent gravitropic responses are known to function in outermost epidermal tissues, whereas auxin-independent AGO component *EGT1* functions in root cortical tissues temporally in basal meristem and transition zone. Dark and light blue color indicates the intensity of *EGT1* expression in these tissues and zones. We propose that EGT1 transcriptionally regulates peroxidases and cell wall loosening machinery and cell wall stiffness in root cortical tissues to counter gravitropic response to determine the gravitropic set point angle.

920

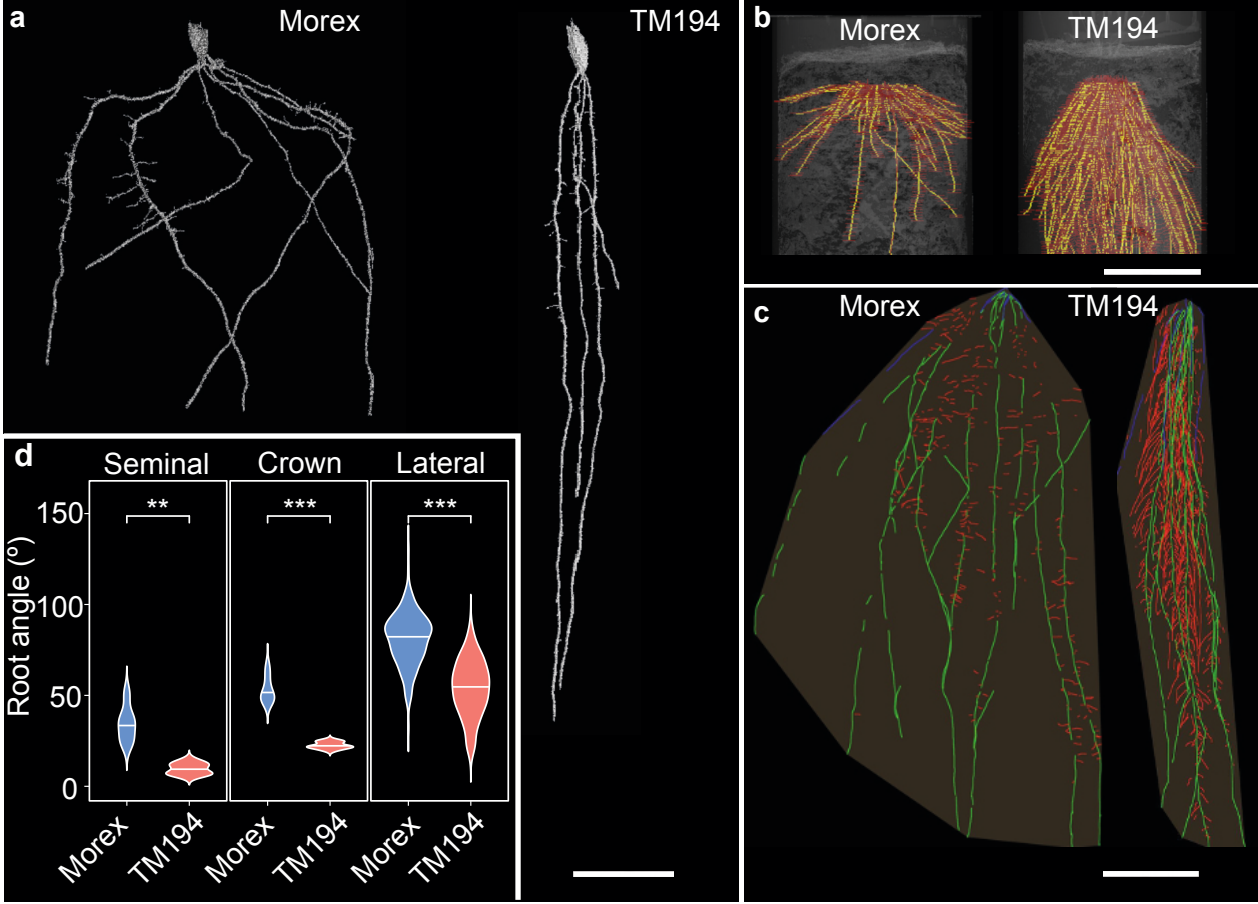
a
Morex
TM194
b
Morex
TM194
c
Morex
TM194
d
Seminal
Crown
Lateral
**
***
***
Root angle (°)
150
100
50
0
Morex
TM194
Morex
TM194
Morex
TM194

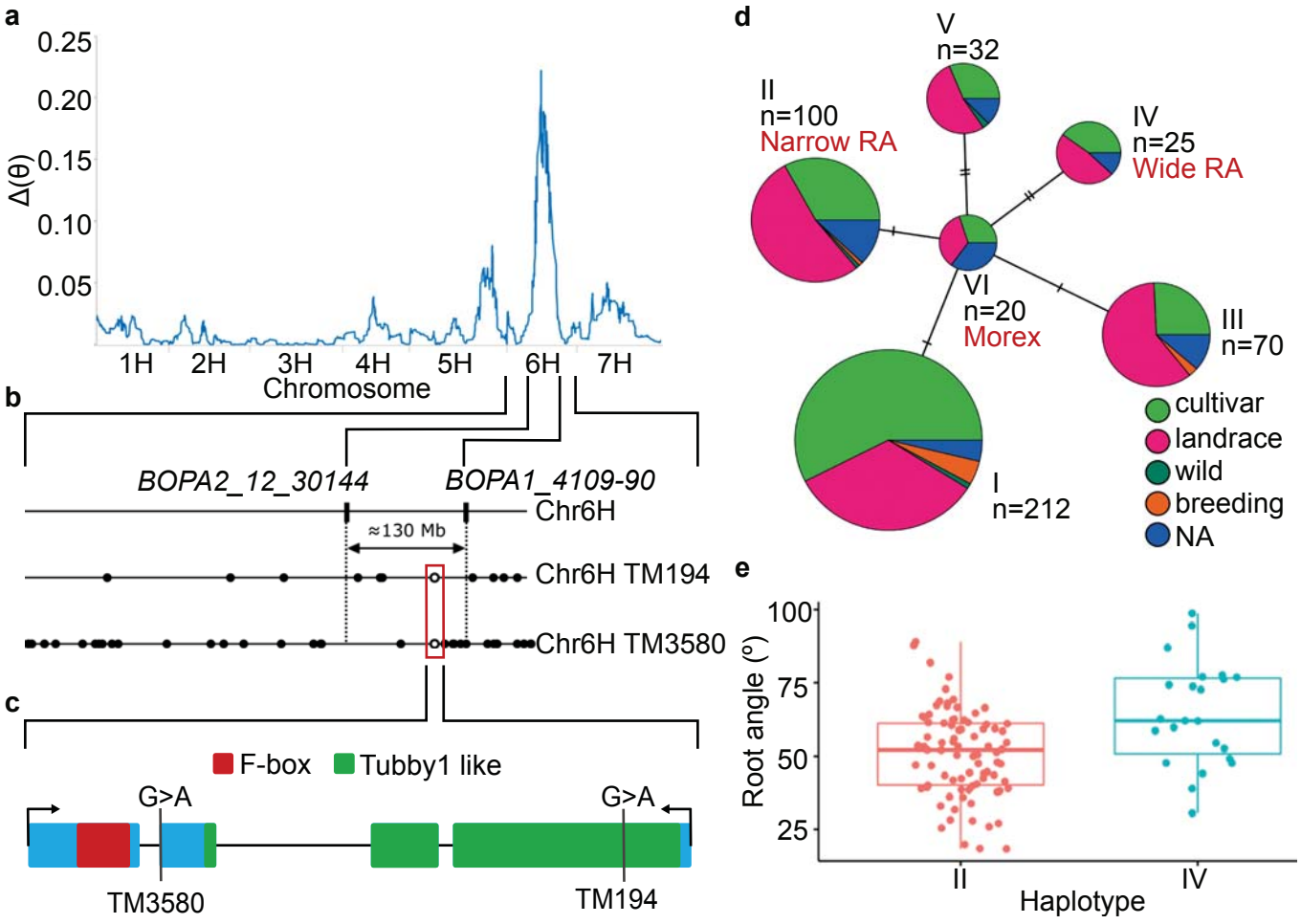
a
0.25
0.20
0.15
0.10
0.05
Δ(θ)
1H
2H
3H
4H
5H
6H
7H
Chromosome
b
BOPA2_12_30144
BOPA1_4109-90
Chr6H
≈130 Mb
Chr6H TM194
Chr6H TM3580
c
F-box
Tubby1 like
G>A
G>A
TM3580
TM194
d
V
n=32
II
n=100
Narrow RA
IV
n=25
Wide RA
VI
n=20
Morex
III
n=70
I
n=212
cultivar
landrace
wild
breeding
NA
e
100
75
50
25
Root angle (°)
II
IV
Haplotype

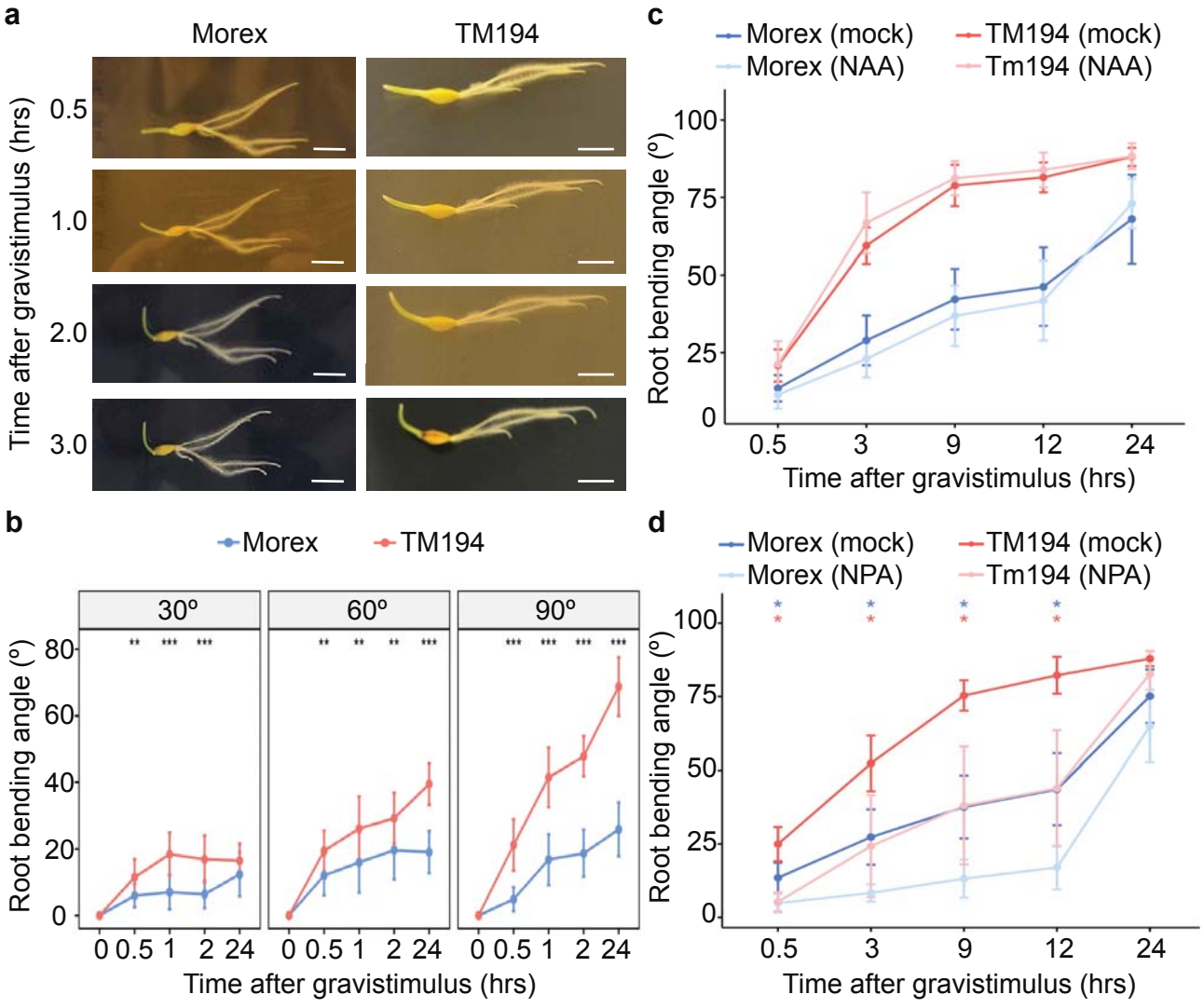
a
Morex
TM194
Time after gravistimulus (hrs)
0.5
1.0
2.0
3.0
b
Morex
TM194
30°
60°
90°
Root bending angle (°)
0 0.5 1 2 24
Time after gravistimulus (hrs)
c
Morex (mock)
TM194 (mock)
Morex (NAA)
Tm194 (NAA)
Root bending angle (°)
0.5 3 9 12 24
Time after gravistimulus (hrs)
d
Morex (mock)
TM194 (mock)
Morex (NPA)
Tm194 (NPA)
Root bending angle (°)
0.5 3 9 12 24
Time after gravistimulus (hrs)

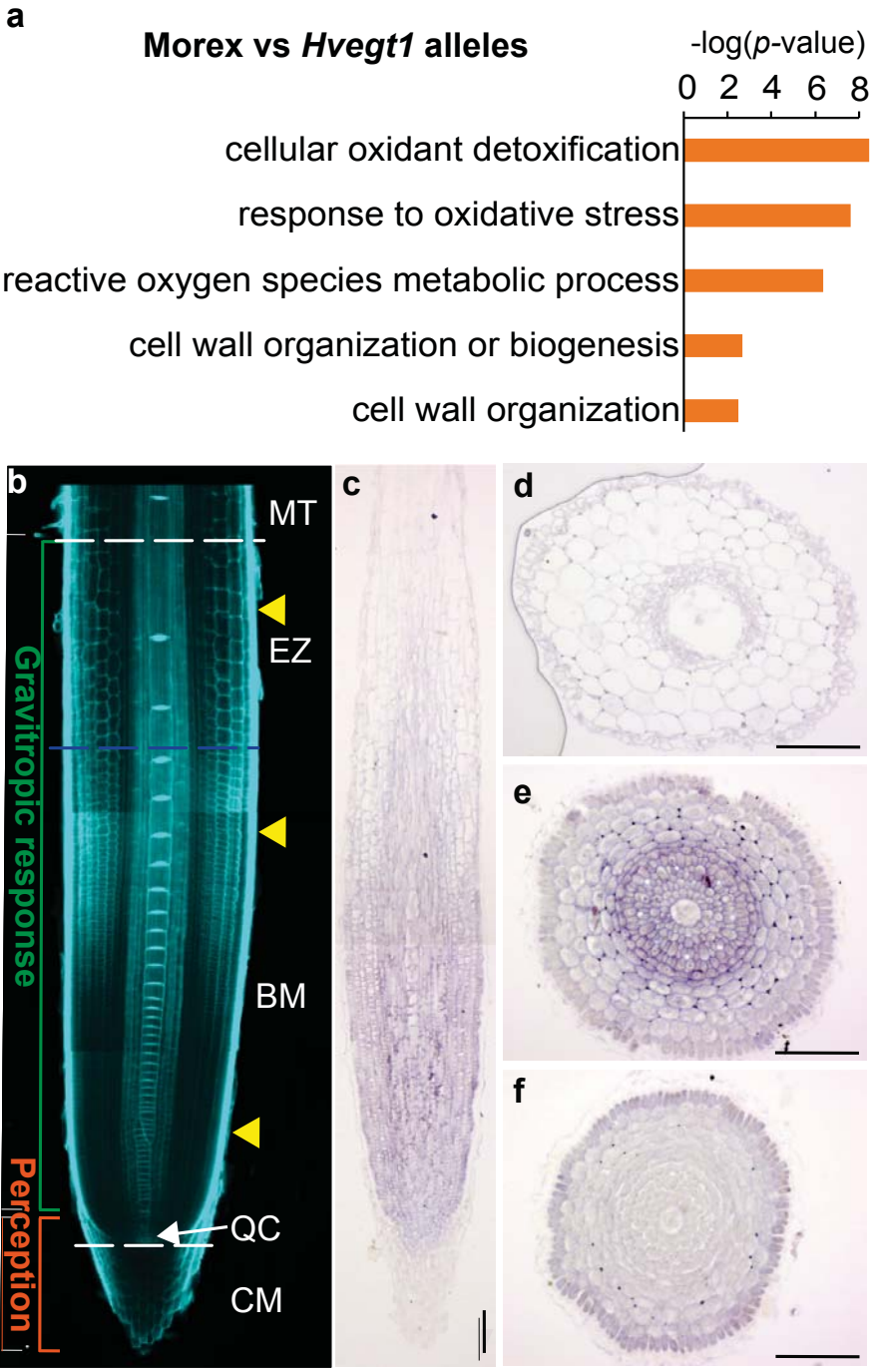
a
Morex vs Hvegt1 alleles
-log(p-value)
0 2 4 6 8
cellular oxidant detoxification
response to oxidative stress
reactive oxygen species metabolic process
cell wall organization or biogenesis
cell wall organization
b
MT
EZ
BM
QC
CM
Gravitropic response
Perception
c
d
e
f
g
30
20
10
0
Stiffness (pN/nm)
***
Morex
TM194
h
epidermis
cortex
stele
cortex
epidermis
AGO response
EGT1
Gravitropic response
Auxin
c
g
EGT1
Regulation of peroxidases & cell wall loosening enzymes
Stiffened cell wall
Anti-gravitropic response